

## Article

# How Is Ultrasonic-Assisted CO<sub>2</sub> EOR to Unlock Oils from Unconventional Reservoirs?

Hengli Wang<sup>1,2</sup>, Leng Tian<sup>1,2,\*</sup>, Kaiqiang Zhang<sup>3,\*</sup>, Zongke Liu<sup>1,2</sup>, Can Huang<sup>1,2</sup>, Lili Jiang<sup>1,2</sup> and Xiaolong Chai<sup>1,2</sup>

- <sup>1</sup> State Key Laboratory of Petroleum Resources and Prospecting, China University of Petroleum (Beijing), Beijing 102249, China; 2018312069@student.cup.edu.cn (H.W.); lzk@cup.edu.cn (Z.L.); 2019310172@student.cup.edu.cn (C.H.); 2021310152@student.cup.edu.cn (L.J.); 2019310171@student.cup.edu.cn (X.C.)
- <sup>2</sup> Department of Petroleum Engineering, China University of Petroleum (Beijing), Beijing 102249, China
- <sup>3</sup> Department of Chemical Engineering, Imperial College London, South Kensington Campus, London SW7 2AZ, UK
- \* Correspondence: tianleng2008@126.com (L.T.); kaiqiang.zhang@imperial.ac.uk (K.Z.); Tel.: +86-10-8973-3740 (L.T.); +44-(0)7742200006 (K.Z.)

**Abstract:** CO<sub>2</sub> enhanced oil recovery (EOR) has proven its capability to explore unconventional tight oil reservoirs and the potential for geological carbon storage. Meanwhile, the extremely low permeability pores increase the difficulty of CO<sub>2</sub> EOR and geological storage processing in the actual field. This paper initiates the ultrasonic-assisted approach to facilitate oil–gas miscibility development and finally contributes to excavating more tight oils. Firstly, the physical properties of crude oil with and without ultrasonic treatments were experimentally analyzed through gas chromatography (GC), Fourier-transform infrared spectroscopy (FTIR) and viscometer. Secondly, the oil–gas minimum miscibility pressures (MMPs) were measured from the slim-tube test and the miscibility developments with and without ultrasonic treatments were interpreted from the mixing-cell method. Thirdly, the nuclear-magnetic resonance (NMR) assisted coreflood tests were conducted to physically model the recovery process in porous media and directly obtain the recovery factor. Basically, the ultrasonic treatment (40 KHz and 200 W for 8 h) was found to substantially change the oil properties, with viscosity (at 60 °C) reduced from 4.1 to 2.8 mPa·s, contents of resin and asphaltene decreased from 27.94% and 6.03% to 14.2% and 3.79%, respectively. The FTIR spectrum showed that the unsaturated C–H bond, C–O bond and C≡C bond in macromolecules were broken from the ultrasonic, which caused the macromolecules (e.g., resin and asphaltenes) to be decomposed into smaller carbon-number molecules. Accordingly, the MMP was determined to be reduced from 15.8 to 14.9 MPa from the slim-tube test and the oil recovery factor increased by an additional 11.7%. This study reveals the mechanisms of ultrasonic-assisted CO<sub>2</sub> miscible EOR in producing tight oils.

**Keywords:** ultrasonic; carbon dioxide; enhanced oil recovery; unconventional reservoirs



**Citation:** Wang, H.; Tian, L.; Zhang, K.; Liu, Z.; Huang, C.; Jiang, L.; Chai, X. How Is Ultrasonic-Assisted CO<sub>2</sub> EOR to Unlock Oils from Unconventional Reservoirs? *Sustainability* **2021**, *13*, 10010. <https://doi.org/10.3390/su131810010>

Academic Editor: Adam Smoliński

Received: 2 August 2021

Accepted: 31 August 2021

Published: 7 September 2021

**Publisher's Note:** MDPI stays neutral with regard to jurisdictional claims in published maps and institutional affiliations.



**Copyright:** © 2021 by the authors. Licensee MDPI, Basel, Switzerland. This article is an open access article distributed under the terms and conditions of the Creative Commons Attribution (CC BY) license (<https://creativecommons.org/licenses/by/4.0/>).

## 1. Introduction

The process of CO<sub>2</sub> flooding has proven to be an effective enhanced oil recovery (EOR) method in unconventional reservoirs [1–4]. The performance of CO<sub>2</sub> miscible flooding is much better than CO<sub>2</sub> immiscible flooding because CO<sub>2</sub> can be dissolved in large quantities in crude oil and reduce the viscosity of the crude oil to improve the recovery in low-permeability reservoirs [5]. Since CO<sub>2</sub> is prone to gas channeling in low permeability reservoirs, it will lead to a low gas utilization rate, and much lower recovery rate of non-miscible flooding than that of miscible flooding [6–8]. However, the high minimum miscible pressure (MMP) of low permeability reservoirs in China makes it difficult to achieve miscible displacement [9]. Therefore, it is of practical and fundamental importance to study promoting CO<sub>2</sub> miscible flooding in low permeability reservoirs by ultrasonic waves.

Reducing MMP is a common method to realize CO<sub>2</sub> miscible flooding [10,11]. The purity of injected CO<sub>2</sub>, the viscosity of formation crude oil, formation temperature, the composition of crude oil, and pore size are all influencing factors of MMP [12–15]. The main direction of reducing MMP between crude oil and CO<sub>2</sub> is to change the properties of carbon dioxide and crude oil [16–19]. During experiments, CO<sub>2</sub> is usually injected into the core together with a certain ratio of liquefied gas, light components of crude oil or other miscible solvents (multi-component petroleum ether, methanol, ethanol, etc.) to promote the dissolution of CO<sub>2</sub> and crude oil to form a miscible displacement layer, reduce the MMP, and improve oil recovery [20–22]. However, due to the consideration of safety and economy, 99.9% CO<sub>2</sub> is injected into the reservoir instead of co-injection of mixed solvents [23]. Therefore, reducing the MMP by changing the nature of CO<sub>2</sub> still has great challenges in application.

Reducing MMP by adding chemicals to reduce the interfacial tension between crude oil and CO<sub>2</sub> is an emerging technology that can improve oil recovery by up to 10% by converting the gas injection process from immiscible to miscible under the same reservoir conditions [24–26]. Mohamed Almobarak et al. confirmed that promising MMP reduction of 9% using 5 wt % of the surfactant-based chemical (SOLOTERRA ME-6) at 373 K by experiment [27]. Zhao found that the MMP can be reduced from 29.6 MPa to 24.1 MPa and the oil recovery efficiency can be increased by 10.3% with the size of citrate acid slug being 0.003 PV into the core [28]. Luo found that compared to ethanol, non-ionic surfactant can significantly reduce the interfacial tension between CO<sub>2</sub> and crude oil. At a dosage of 0.5 wt %, it causes far higher reduction of the IFT than 20 wt % pentane or 5 wt % ethanol; the MMP and the first-contact miscibility pressures (P-max) of the crude oil/CO<sub>2</sub> systems were decreased from 19.1 and 43.0 to 13.8 and 19.0 MPa, respectively [29]. The method of injecting chemicals can effectively reduce the MMP and improve the efficiency of CO<sub>2</sub> flooding, but environmental protection restricts the large-scale application of chemicals.

In recent years, ultrasonic has attracted wide attention from scholars for its environmental friendliness and remarkable production-increasing effect [30–33]. The heat generation, vibration, cavitation, and emulsification of ultrasonic waves can reduce the viscosity of crude oil, and the capillary force and surface tension of oil and water in the process of water flooding, thereby improving the flow capacity of crude oil, which are the most important mechanisms that improve oil recovery factor [34–36]. Hossein Hamidi [37] verified an exciting finding that improving oil recovery by combining ultrasound application with CO<sub>2</sub> flooding could be beneficial. However, he only analyzed the effect of ultrasonic-assisted CO<sub>2</sub> flooding temperature on oil recovery through experimental methods and determined the optimal CO<sub>2</sub> injection rate. He neither did in-depth analysis on the mechanism of EOR enhancement nor did he determine whether MMP could reduce the effect of ultrasound. So far, there has been no experimental attempt to determine how ultrasonic action reduces MMP and enhances recovery.

This study aims to analyze the effect of ultrasonic-assisted CO<sub>2</sub> flooding on MMP, pore structure, and crude oil viscosity by combining slim tube experiment, NMR, infrared spectroscopy, viscosity test, and displacement experiment. Besides, it tries to explain the mechanism of enhanced oil recovery by ultrasonic-assisted CO<sub>2</sub> flooding and provide a basic theoretical basis for the wide range application of ultrasonic-assisted CO<sub>2</sub> flooding in oil fields in the future.

## 2. Materials and Methods

### 2.1. Materials

The samples obtained for this study were derived from tight sandstone samples sandwiched by the Upper Triassic Yanchang Formation in the JiYuan area located in the central Ordos Basin, China. For the core, its length is 10.2 cm, the diameter is 2.5 cm, the permeability is 1.56 mD, and the porosity is 10.3%. It belongs to a low permeability reservoir according to permeability. The oil samples were collected from the surface degassing crude oil of the Chang 6 low permeability reservoir in Ordos Basin. The density and viscosity

of the oil sample were  $895 \text{ kg/m}^3$  and  $3.8 \text{ mPa}\cdot\text{s}$  at  $60 \text{ }^\circ\text{C}$  (Reservoir temperature) and atmospheric pressure, respectively. The purity of  $\text{CO}_2$  used in the experiment was 99.9%.

## 2.2. Equipment Setup

### 2.2.1. Subsubsection

The oil viscosity, oil component, and functional group were measured by viscometer, gas chromatography, and Fourier-transform infrared spectroscopy (FTIR). The viscometer used in this experiment was VISCOLab PVT produced by Cambridge Viscometer Co., Ltd., Houston, Texas, USA. The maximum test pressure is 138 MPa, the maximum temperature is  $190 \text{ }^\circ\text{C}$ , the measurement range is 0.02–10,000 CP, and the measurement error is 1%. Total hydrocarbon analysis was performed using Agilent 7890 gas chromatography-mass spectrometer. The stationary phase of the high resolution chromatographic column is a quartz capillary column formed by the crosslinking of polydimethylsiloxane. The column length is 35–50 m, the inner diameter is 2.2–2.5 cm, the operating temperature is higher than  $320 \text{ }^\circ\text{C}$ , and the column efficiency is higher than 3000 theoretical plate/m, and the measurement error is 1%. Fourier infrared spectrum instrument is an FT-IR model produced by SPECIM Company in Finland, with a resolution of  $4 \text{ cm}^{-1}$  and a spectral range of  $7800\text{--}350 \text{ cm}^{-1}$ .

### 2.2.2. Slim-Tube Test

In this research, the slim-tube apparatus was used to determine the MMP of the oil and  $\text{CO}_2$  at the constant reservoir temperature. The experimental apparatus is shown in Figure 1, which mainly includes: (1) ISCO pump (Quizix5000, Broken Arrow, OK, USA), which can provide the maximum displacement pressure of 70 MPa for the experiment. (2) Slim tube (from Hai'an, Nantong, China), which has been filled by 160 mesh quartz sand and with an internal diameter of 5 mm, a length of 20 m; the permeability is 1200 mD and the porosity is 22.8%. (3) Ultrasonic bath (Beijing Xiangyu Ultrasonic Industrial Equipment Co., LTD Beijing, China); the ultrasonic waves with a frequency of 40 KHz and a power of 200 W were emitted by transducer transmitted to the slim-tube through the water in the water tank. On the one hand, water is the medium of ultrasonic transmission. On the other hand, the ultrasonic bath can control the temperature of water and keep the experimental temperature constant. (4) Observation window, used to look at miscible states. (5) Backpressure valve (HY-2, Nantong, China), used to stabilize the back pressure to ensure that the displacement pressure difference is stable. (6) Hand pump, used to provide pressure to the backpressure valve. (7) Measuring device; the produced oil was monitored and measured by an electronic balance with an accuracy of 0.0001 g.

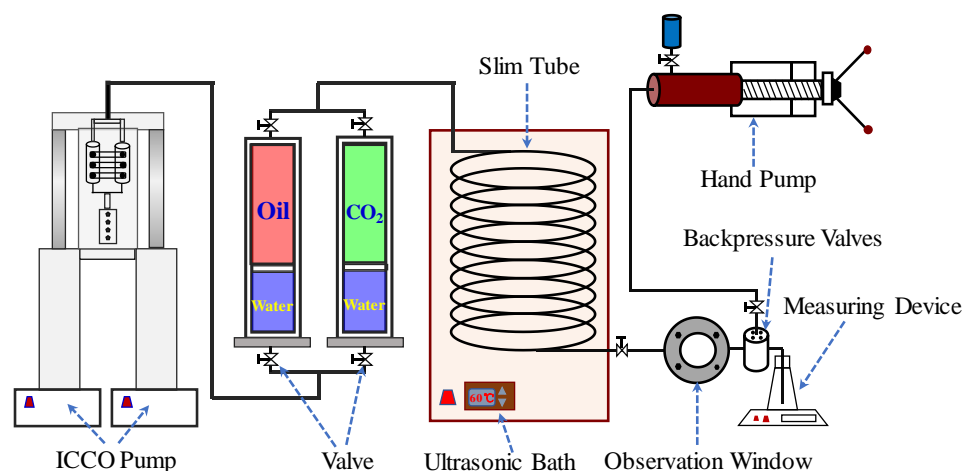


**Figure 1.** Experimental installation diagram of thin tube.

### 2.2.3. NMR and CO<sub>2</sub> Flooding

The experimental setup for the ultrasonic-assisted CO<sub>2</sub> flooding and on-line NMR testing is shown in Figure 2. It consists of four subsystems, i.e., displacement subsystem with nuclear magnetic resonance, ultrasonic generation subsystem, measuring subsystem, and assistant subsystem. In the displacement subsystem, the ICSO pump (Broken Arrow, OK, USA) can provide the maximum displacement pressure of 70 MPa for the experiment; the pressure passed from the pump ICSO pushes the fluid in the container (Hai'an, Nantong, China) to the core holder (from Hai'an, Nantong, China, with diameter of 26 mm, length of 90–150 mm) and it flows through the core to the vent. Two hand pumps (P5, 35 MPa, 80 °C, Oxford, UK) provide confining pressure to the core holder and pressure to the backpressure valve (HY-2, Nantong, China). The NMR instrument (from Oxford instruments, UK; the radio frequency is distributed in a range of 1–30 MHz with a control precision of 0.1 MHz. Besides, the echo time is set to be 0.12 ms, the waiting time is 1.125 s for measurement, and the scanning number is 32) is used to detect the spectrum of transversal relaxation time ( $T_2$ ) to analyze the recovery of CO<sub>2</sub> flooding and residual oil distribution. The ultrasonic generation subsystem consists of an ultrasonic generator (HC-SG-202000, from Hangzhou, China, with 40 KHz and 50 W) and a transducer. The measuring subsystem consists of a high-precision electronic balance and a gas flow meter (50 scm, Alicat Scientific Inc., Tucson, Arizona, USA). As an assistant subsystem, the thermotank (from Hai'an, Nantong, China) can maintain the experimental temperature from room temperature range to 120 °C, with an error of  $\pm 1$  °C.

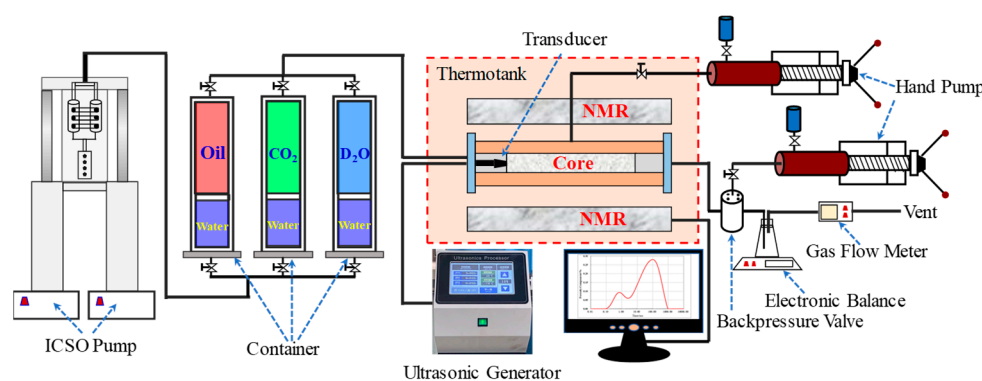


**Figure 2.** Diagram of ultrasonic-assisted CO<sub>2</sub> displacement device.

## 2.3. Procedure

### 2.3.1. Physical Property Measurement

The changes of oil viscosity, group component, composition, and functional groups after ultrasonic treatment have been measured. 1 L crude oil was averagely divided into two parts with the same viscosity, composition, and functional group. One part of them is used for viscosity test, gas chromatography test and infrared spectroscopy test. The other part of the crude oil is sealed in the glass beaker, then the beaker is completely submerged under the water surface of the ultrasonic bath. The crude oil was treated with 40 KHz and 50 W ultrasonic waves for 8 h and then left for 6 h at 20 °C and atmospheric pressure to measure viscosity, gas chromatography, and infrared spectroscopy.

The viscosity–temperature curves of crude oil viscosity changing with temperature were obtained in the temperature range of 20–60 °C. Group components include saturated hydrocarbons, aromatic hydrocarbons, resins, asphaltenes (SARA). The filtrate formed by asphaltene precipitation in crude oil was separated by a silica–alumina column with n-hexane and then saturated hydrocarbon, aromatic hydrocarbon, and resin components were leached out by dichloromethane, anhydrous ethanol, and chloroform, respectively. The contents of four kinds of components were obtained by weighing the weight of the solvent after volatilization.

During the analysis of crude oil by gas chromatography, the gasified oil sample was first slowly passed through capillary column with carrier gas to separate light hydrocarbons less than  $C_8$  and alkanes from  $C_8$ - $C_{40}$ . The concentration of each component was detected by the flame ionization detector and the mass fraction of each component was calculated by the area normalization method. The capillary column temperature was stabilized at  $40\text{ }^\circ\text{C}$  for 10 min and then raised to  $320\text{ }^\circ\text{C}$  at  $5\text{ }^\circ\text{C}/\text{min}$ . The temperature of the vaporization chamber and detection chamber was kept at  $330\text{ }^\circ\text{C}$  and the split ratio was controlled at 1:40–1:120. The linear velocity of helium is 20 cm/s, the flow rate of hydrogen gas is 30 mL/min, and air flow rate is 300 mL/min. After the instrument was stabilized, 0.2–1.0  $\mu\text{L}$  samples were extracted with a microinjector. At the same time, the programmed temperature was started, and the chromatographic processor was used to record the chromatogram and original data.

After adjusting the sensitivity, parameter mode, gain, and velocity of the infrared spectrometer, the infrared analysis begins. First, the potassium bromide slide was cleaned with anhydrous ethanol, and background data was measured for later reference. Then, the crude oil was evenly smeared on the slide, the C-H vibration response of the absorption spectrum was adjusted to 100%, and the absorption peak heights of methyl, methylene, aromatic ring, and carbon and oxygen functional groups were taken as their relative contents for quantitative calculation.

### 2.3.2. Slim-Tube Test

Once the slim tube is saturated with the crude oil sample at  $60\text{ }^\circ\text{C}$ ,  $\text{CO}_2$  is introduced to displace the oil at an injection rate of  $0.2\text{ cm}^3/\text{min}$ . The volume of oil produced after the  $\text{CO}_2$  injection volume reaches 1.2 PV at displacement pressure of 12 MPa, 14 MPa, 15 MPa, 16 MPa, 18 MPa, and 20 MPa was recorded respectively. The displacement pressure difference was 0.5 MPa. Keeping the experimental material, temperature, pressure the same and repeating the above experimental procedure while the ultrasonic bath machine was open, the MMP of ultrasonic-assisted  $\text{CO}_2$  flooding was measured.

### 2.3.3. NMR and $\text{CO}_2$ Flooding

- Step #1: After the gas permeability measurement of core samples was completed, the sample was vacuum pressurized (15 MPa) with saturated brine and placed in the core holder in Figure 2 for the NMR test.
- Step #2: The sample was dried and the brine made of deuterium oxide with purity of 99.99% was saturated by vacuum pressure (15 MPa). Then, the crude oil was saturated by the displacement method with the displacement pressure 16 MPa, the displacement pressure difference 1 MPa, and the confining pressure 18 Mpa. Stop injecting crude oil if the outlet does not produce water for an hour in a row, and the remaining water in the core is bound water that cannot flow. Then, the core sample was placed in the core gripper and aged with confining pressure for 120 h for NMR test.
- Step #3: The samples were replaced with  $\text{CO}_2$  at a displacement pressure of 15 MPa, displacement pressure difference of 1 MPa and confining pressure of 17 MPa. Record oil and gas production data, respectively. When the injection volume of  $\text{CO}_2$  reached 1.6 PV, the displacement experiment was stopped for the NMR test.
- Step #4: The residual oil in the pores was thoroughly washed by the solution prepared with alcohol and benzene at a volume ratio of 1:3, then dried at  $105\text{ }^\circ\text{C}$  for 12 h. Repeat step #2.
- Step #5: Open the ultrasonic generator, repeat step #3, measure ultrasonic-assisted  $\text{CO}_2$  displacement recovery.

## 3. Results and Discussion

### 3.1. Oil Physical Properties

Table 1 shows the changes of group composition after ultrasonic treatment for 8 h. It can be seen from the table that the contents of saturated hydrocarbon and aromatic

hydrocarbon in crude oil increased by 9.8% and 6.2% after ultrasonic treatment, and the contents of resin and asphaltene decreased by 13.7% and 2.2%, respectively. The experimental results show that the crude oil treated by ultrasonic is cracked, and the heavy components such as gum and asphaltene in crude oil are transformed into light components such as saturated hydrocarbons and aromatic hydrocarbons.

**Table 1.** SARA of ultra-oil samples before and after ultrasonic treatment.

	Saturated Hydrocarbon/%	Aromatic Hydrocarbon/%	Resin/%	Asphaltene/%
Without ultrasonic	52.38	13.65	27.94	6.03
With ultrasonic	62.15	19.87	14.20	3.79

Figure 3 is the result of gas chromatography. The results show that after ultrasonic treatment for 8 h, the molar percentage of  $C_{25}$ - $C_{30+}$  in crude oil decreases, which means that the content of heavy hydrocarbon molecules decreases, and the decrease of  $C_{30+}$  component is the largest, from 5.6% to 5.0%. With the decrease of C atom number, the decrease of molar percentage is also reduced. However, the  $C_{12}$ - $C_{24}$  mole percentage increases, and  $C_3$ - $C_{11}$  changes irregularly. The experimental results show that the heavy hydrocarbon molecules ( $C_{25+}$ ) in crude oil components can be decomposed into medium hydrocarbon molecules ( $C_{12}$ - $C_{24}$ ) by ultrasound. Studies have shown that the MMP is related to the content of heavy hydrocarbon molecules in crude oil. The greater the content of heavy hydrocarbon molecules is, the greater the MMP is [38–40]. This is one of the important reasons why ultrasound can reduce MMP.

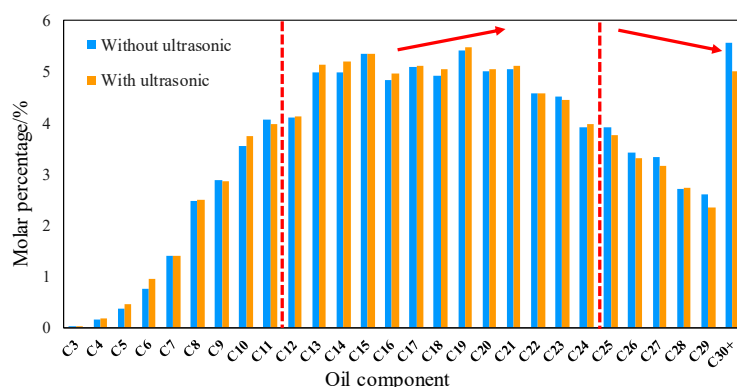


**Figure 3.** Result of gas-chromatography experiment (the mole fraction of  $C_{25+}$  goes down, the mole fraction of  $C_{12-24}$  goes up).

Cavitation is the main mechanism of ultrasonic changing crude oil composition. Cavitation gathers ultrasonic energy in the tiny space of crude oil to form tiny bubbles called the nucleus. When the cavitation nucleus disappears, it produces huge pressure and releases a lot of heat. The high temperature and high pressure around the cavitation core and the accompanying severe mechanical shear can improve the activity of crude oil macromolecules, start the thermal decomposition reaction similar to combustion, and thus break the crude oil macromolecules into small molecules [41,42].

Infrared spectroscopy is one of the main methods for identifying functional groups and molecular structures of substances. The infrared spectrum is the characteristic absorption peak of typical hydrocarbon (functional group). The functional groups in crude oil samples can be sensitively studied by Fourier transform infrared spectroscopy, and the relative concentration (ratio) of each functional group can be obtained by the relative quantitative calculation of aromatic rings, methylene and methyl according to the peak height or area. By comparing and analyzing the infrared spectra of crude oil before and after the reaction,

the changes of various functional groups and their relative contents in the samples can be revealed [43,44].

The FTIR spectrum covers the range of 4000–400  $\text{cm}^{-1}$ . The region in 700–820  $\text{cm}^{-1}$  presents the out-plane bending vibration of C-H structure and the region in 1000–1100  $\text{cm}^{-1}$  shows the stretching vibration of C-O structure. There are double peaks that the peak areas are equal with; values are 1365  $\text{cm}^{-1}$  and 1395  $\text{cm}^{-1}$  in the range of 1340–1410  $\text{cm}^{-1}$ , which presents the in-plane bending vibration of C-H structure [45]. In the range of 1560–1620  $\text{cm}^{-1}$ , 1620–1680  $\text{cm}^{-1}$  shows the stretching vibration of C=C groups; interestingly, 1560–1620  $\text{cm}^{-1}$  represents the C=C stretching vibration of aromatic molecules, while 1620–1680  $\text{cm}^{-1}$  is the C=C structure of alkenes [46]. The ranges of 2010–2070  $\text{cm}^{-1}$  and 2920–2980  $\text{cm}^{-1}$  indicate the stretching interval of  $\text{C}\equiv\text{C}$  and  $-\text{CH}_2-$ , respectively. The range of 3300–3500  $\text{cm}^{-1}$  shows the stretching vibration of C-H [47,48].

Figure 4 shows the test results of FTIR. The red line represents the infrared absorption spectrum of crude oil without ultrasonic treatment, and the blue line represents the infrared absorption spectrum of crude oil after 8 h of ultrasonic treatment. The origin 2018 software (Origin Lab Corp., Northampton, MA, USA) was used to segment fit the peak values of the infrared spectrum, and the area of each peak area was obtained to represent the number of corresponding functional groups. The results are shown in Table 2. After ultrasonic treatment, the peak areas of both in-plane bending vibration and out-of-plane bending vibration of saturated C-H increased, and in addition, the peak areas of unsaturated C-H stretching vibration decreased, that is to say, the unsaturated C-H bond was broken and turned into a saturated C-H bond due to ultrasonic treatment. Because the unsaturated C-H bond mainly exists in colloid and asphaltene, it can be inferred that the unsaturated C-H bond of colloid and asphaltene is mainly cracked by ultrasonics, converted to saturated C-H bond by hydrogenation reaction. The decrease of the number of C-O functional groups indicates that the C-O bond in crude oil is broken by ultrasonic, and hydrogen atoms replace oxygen atoms to bond with carbon atoms, which is one of the reasons for the increase in the number of C-H functional groups. With the ultrasonic treatment, the number of the  $\text{C}\equiv\text{C}$  bond decreases, and the C=C bond in both aromatic ring and olefin increases, indicating that the  $\text{C}\equiv\text{C}$  bond was cracked into the C=C bond by ultrasonic treatment. In summary, the ultrasonic action makes the C-H bond, C-O bond, and  $\text{C}\equiv\text{C}$  bond of resin and asphaltene in crude oil crack to generate the C-H bond and C=C bond of saturated hydrocarbon and aromatic hydrocarbon.

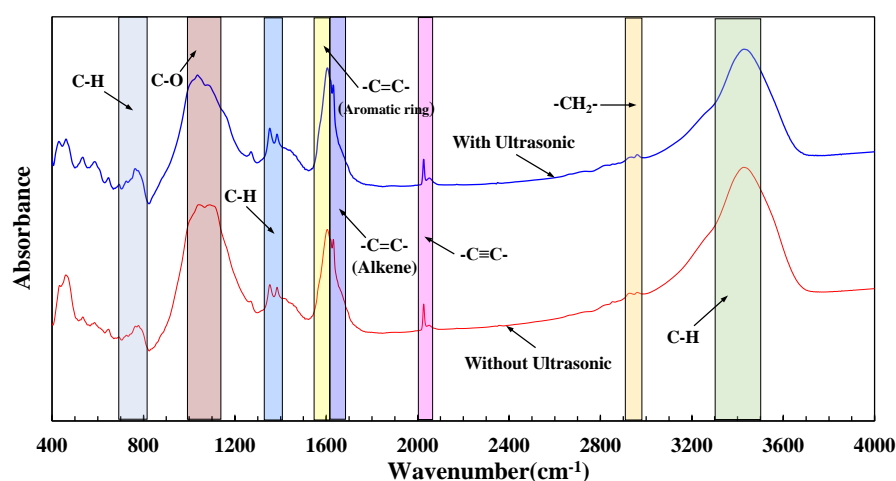
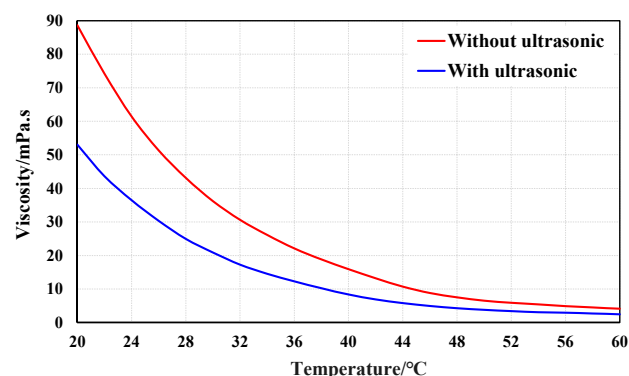


Figure 4. Result of FTIR.

**Table 2.** Number of functional groups of ultra-oil samples before and after ultrasonic treatment.

Functional Groups	C-H (Out-Plane Bending Vibration)	C-O	C-H (In-Plane Bending Vibration)	C=C (Aromatic Ring)	C=C (Alkene)	C≡C	-CH <sub>2</sub>	C-H (Stretching Vibration)
Range/cm <sup>-1</sup>	700–820	1000–1100	1340–1410	1560–1620	1620–1680	2010–2070	2920–2980	3300–3500
Area (Without ultrasonic)	23.27	78.56	20.58	8.78	15.11	4.38	1.82	96.3
Area (With ultrasonic)	26.74	70.21	21.35	9.46	16.07	4.07	1.81	88.7

The viscosity test results in Figure 5 shows that the crude oil's viscosity decreases with the increase of temperature. When the temperature is less than 44 °C, the viscosity decreases greatly with the increase of the temperature, but it decreases gently afterwards. After the ultrasonic wave process, the viscosity of crude oil decreases from 88.6 mPa·s to 53.1 mPa·s at 20 °C, and decreases from 4.1 mPa·s to 2.5 mPa·s at 60 °C. Resin and asphaltene are the most important factors for controlling the viscosity of crude oil. With asphaltenes as the core, resins are attached to asphaltenes to form aggregates or micelles which are dispersed in the dispersion medium composed of light components and some resins. The connection between resin and asphaltenes was destroyed by the ultrasonic treatment, which makes the micelle structure loose and reduces the cohesion between crude oil molecules, which is shown by the decrease of the crude oil viscosity. With no ultrasonic treatment, the crude oil contains 33.97% of the heavy components of resin and asphaltene, which suggests the characteristics of high viscosity. After ultrasonic treatment, the total content of resin and asphaltene in crude oil decreased to 17.99%, which was the main reason for the ultrasonic process reducing the viscosity of the crude oil.



**Figure 5.** Viscosity–temperature curve of ultra-oil samples before and after ultrasonic treatment (in the absence of the ultrasonic effect, the oil viscosity was 88.6 mPa·s at 20 °C and 4.1 mPa·s at 60 °C; the viscosity of crude oil was 53.1 mPa·s at 20 °C and 2.5 mPa·s at 60 °C after 8 h of ultrasonic treatment).

### 3.2. Miscibility Development

The experimental results of the slim-tube are shown in Figure 6. It can be seen that the experimental results of the tube can be demonstrated by two straight lines. The pressure corresponding to the intersection point of the straight line is the MMP. Without ultrasonic, the MMP was 15.9 MPa but with ultrasonic, it fell to 14.8 MPa, indicating that ultrasonic treatment can reduce the MMP between CO<sub>2</sub> and crude oil. With the ultrasonic wave, the oil recovery can be improved by 8.9%, while the pressure for displacement can be increased by 12 MPa. The increase of recovery rate decreases gradually with the increase of injection pressure, especially when the pressure is greater than the MMP, and the increase of recovery rate decreases rapidly. Only 0.6% recovery can be increased by ultrasonic when the displacement pressure is 20 MPa. It can be seen that the ultrasonic is the best way to improve the development of CO<sub>2</sub> immiscible flooding since the recovery ratio of miscible

flooding in the slim tube experiment is greater than 90%, and there is little residual oil used to improve the recovery ratio.

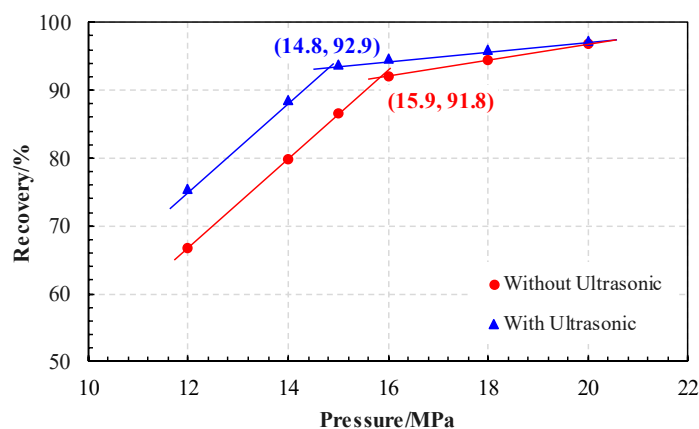


**Figure 6.** Result of slim-tube test (the MMP decreased from 15.9 MPa without ultrasonic to 14.8 MPa after ultrasonic treatment for 8 h).

A large number of studies have shown that the MMP is associated with the purity of injected CO<sub>2</sub>, crude oil composition, reservoir temperature, and the size of pore and throat, and it is most affected by the crude oil composition [11,49–52]. The MMP increases with the increase of the molar fraction of C<sub>11</sub>–C<sub>19</sub> and C<sub>20+</sub> in crude oil, which are almost linearly correlated with MMP. The difference is that MMP increases more with the increase of C<sub>20+</sub>, meaning that the influence of the molar content of C<sub>20+</sub> on MMP is more intense [53]. There are many empirical formulas for calculating the MMP considering the reservoir temperature, crude oil composition, and gas composition [54–58]. Among them, the method of characteristic theory and the mixing-cell method is one of the most classical methods for calculating MMP. Ge et al. [13] proposed a prediction model for CO<sub>2</sub>–oil MMP, which considered multi-stage contact based on the method of characteristic theory and the mixing-cell method. This method is used to calculate the MMP of the CO<sub>2</sub>–oil system before and after ultrasonic treatment in this paper. The pressure corresponding to a zero-length tie line is MMP which is acquired by power-law extrapolation, but the extrapolation can also lead to the error of prediction. Therefore, Ge et al. proposed to approximate the MMP with the minimum value of the characteristic curve. The calculation formula for the minimum value of the characteristic curve is:

$$V_{\min} = 0.0017 \times T + 0.057 \times C_{7-15} + 0.174 \times C_{16-26} - 0.0405 \times C_{27+} \quad (1)$$

where  $V_{\min}$  is the minimum value,  $T$  is reservoir temperature,  $C_{7-15}$  is mole fraction,  $C_{16-26}$  is mole fraction,  $C_{27+}$  is mole fraction. Table 3 shows the calculation parameters and results; the minimum value of the characteristic curve without ultrasonic effect is 0.203, and the minimum value of the characteristic curve with ultrasonic effect is 0.212.

**Table 3.** Calculation parameters and results.

	T/°C	C <sub>7-15</sub> /%	C <sub>16-26</sub> /%	C <sub>27+</sub> /%	V <sub>min</sub>
Without ultrasonic	60	33.82	50.67	15.51	0.203
With ultrasonic	60	34.32	54.44	11.24	0.212

As is shown in Figure 7, mix a cell G filled with injected gas and a cell O filled with crude oil in a certain proportion (typically 50% each). At a fixed temperature and pressure, the composition of the equilibrium gas phase  $Y_1$  and liquid phase  $X_1$  is calculated by negative flash, and the first contact is completed by adding four units of crude oil O and injected gas G. For the second contact, the equilibrium gas phase cell  $Y_1$  continues to mix

with the crude oil cell O in the front, and the equilibrium liquid phase cell  $X_1$  continues to mix with the injected gas cell G in the rear, producing  $X_{21}$ ,  $Y_{21}$ ,  $X_{22}$ , and  $Y_{22}$ . Two groups of equilibrium gas–liquid compositions were obtained by two negative flash calculations; there are 6 cells, including crude oil and injected gas. In this way,  $2n + 2$  cells should be obtained when the  $n$ th contact is completed. The length of the line can be presented by equilibrium components  $X_i, Y_i$ :

$$TL = \sqrt{\sum_{i=1}^{N_c} (x_i - y_i)^2} \tag{2}$$

where  $TL$  is the tie-line length,  $N_c$  is the number of components, and  $X_i$  and  $Y_i$  are liquid and gas equilibrium compositions, respectively.

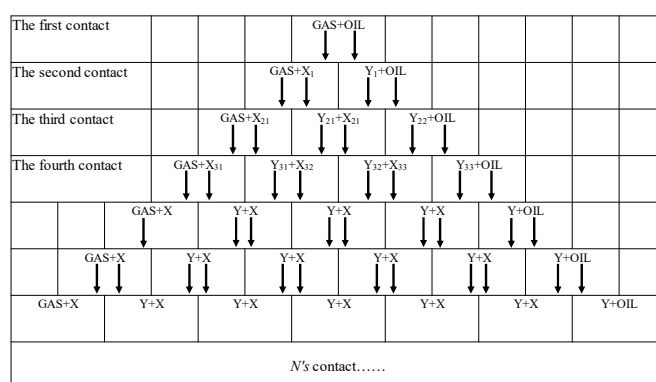


Figure 7. Mixing-cell processes [58].

Firstly, at a fixed reservoir temperature and an initial pressure less than MMP, the gas–liquid equilibrium is calculated by the PR equation of state as shown in Figure 7. After 200 contact times, the gas–liquid tie-line length ( $TL$ ) of each group was calculated, and the minimum tie-line length ( $MTL$ ) was selected. Then, slightly increase the pressure value and repeat the above steps, and the  $MTL$  under the pressure can be calculated. Taking the pressure as the abscissa and the  $MTL$  as the ordinate, the  $MTL$  under all pressure is drawn in the rectangular coordinate system. Figure 8 shows the relationship between the  $MTL$  and pressure. It can be seen from the figure that the  $MTL$  decreases with the increase of pressure. When the pressure is the same, the  $MTL$  with ultrasonic is smaller than the one without ultrasonic.

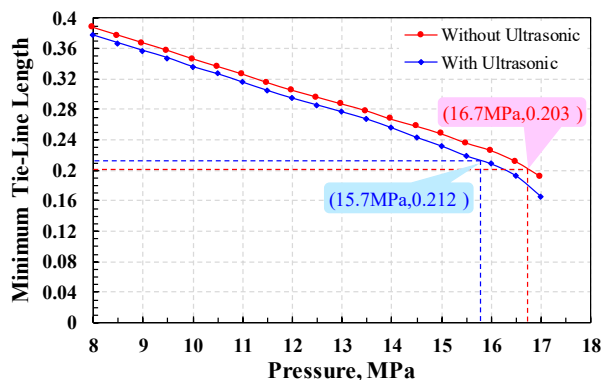
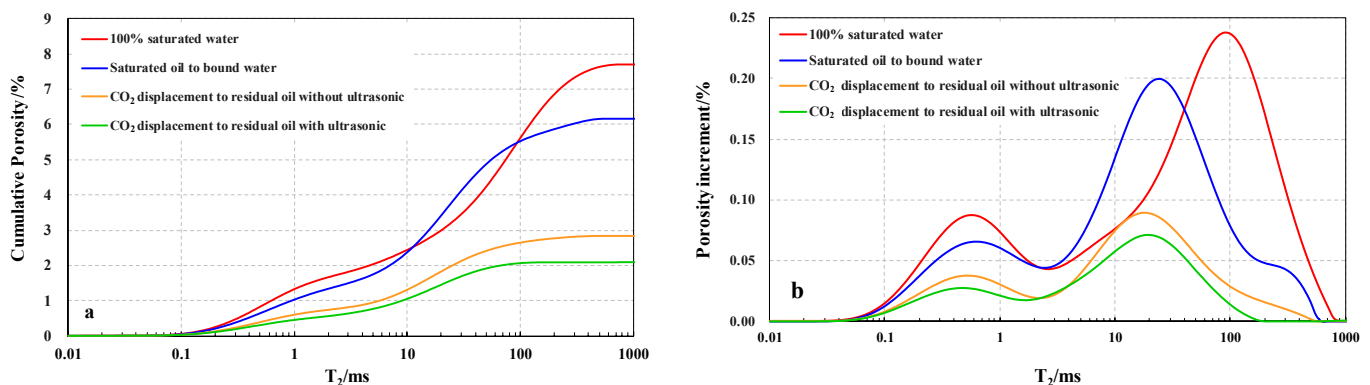


Figure 8. The relationship between  $MTL$  with pressure (with the increase of pressure, the  $MTL$  decreases. Under the same pressure condition, the  $MTL$  of ultrasonic treatment is always smaller than that of non-ultrasonic treatment).

According to Equation (1), the MTL of the CO<sub>2</sub>–oil system without ultrasonic is 0.120, and the corresponding MMP is 16.7 MPa. The MTL of the CO<sub>2</sub>–oil system assisted by ultrasonic is 0.212, and the MMP is 15.7 MPa. Obviously, the MMP of CO<sub>2</sub>–oil system decreases after applying ultrasonic, indicating that the ultrasonic effect can promote the CO<sub>2</sub>–oil system to reach the miscible state.

### 3.3. Oil Recovery

Figure 9a is the cumulative T<sub>2</sub> spectrum distribution curve of CO<sub>2</sub> flooding. The final value of the cumulative T<sub>2</sub> distribution curve for 100% saturated water (the red curve) in Figure 9a represents a core porosity of 7.7%. Since the D<sub>2</sub>O filled in the core before oil saturation can shield the NMR signal [59], the final value of the cumulative T<sub>2</sub> spectrum distribution curve of saturated oil to bound water (the blue curve) represents that the crude oil in the core occupies 6.2% of the core volume. Similarly, the accumulated T<sub>2</sub> spectrum after the CO<sub>2</sub> displacement without the ultrasonic wave (the orange curve) reflects a porosity of 2.8% for the residual oil. After the ultrasonic CO<sub>2</sub> displacement (the green curve), the porosity of the residual oil was 2.1%. According to the information provided in Figure 9a, the initial oil saturation is 80.5%, the residual oil saturation is 36.7% and the recovery is 54.3% without ultrasonic CO<sub>2</sub> displacement. The residual oil saturation of ultrasonic-assisted CO<sub>2</sub> flooding was 27.3%, and the recovery factor was 65.9%. Compared with other unchanged conditions, the ultrasonic-assisted CO<sub>2</sub> flooding has additional recovery after CO<sub>2</sub> flooding by 11.7%. One of the most important reasons is that in the absence of the ultrasonic effect, the MMP obtained by the thin tube experiment is 15.9 MPa, and the CO<sub>2</sub>–oil system is immiscible due to the displacement pressure of 15 MPa being less than the MMP. Ultrasonic-assisted CO<sub>2</sub> displacement reduced the MMP to 14.8 MPa, which promotes the CO<sub>2</sub>–oil system to miscible state, so the recovery is greatly improved.



**Figure 9.** (a) The accumulation T<sub>2</sub> curve of CO<sub>2</sub> flooding ( $\phi = 7.7\%$ , porosity of saturated oil is 6.2%, porosity of residual oil without ultrasonic is 2.8%, and porosity of residual oil with ultrasonic is 2.1%) and (b) the porosity increment T<sub>2</sub> curve of CO<sub>2</sub> flooding.

Figure 9b is the T<sub>2</sub> spectrum curve of the porosity increment of CO<sub>2</sub> flooding. The blue curve represents the T<sub>2</sub> spectrum of the porosity increment of saturated oil to bound water, the orange curve and green curve represent the residual oil in CO<sub>2</sub> flooding without ultrasonic and residual oil in CO<sub>2</sub> flooding with ultrasonic, respectively. The relaxation time of NMR is proportional to the pore radius, which means that the relaxation time can represent the radius of oil droplets in pores for NMR curves of oil signal. The maximum T<sub>2</sub> value of the orange curve is 501 ms, which is similar to the maximum value of the blue curve, indicating that there are still oil droplets with a large radius in the pores after CO<sub>2</sub> displacement without ultrasonic. Cluster residual oil with a large radius is formed due to the difficulty of reaching pores due to CO<sub>2</sub> flow around and breakthrough during CO<sub>2</sub> immiscible flooding. The maximum T<sub>2</sub> value of the green curve is 158 ms, which is far less than the maximum of the orange curve. It shows that the large oil droplets of the residual oil decrease after the CO<sub>2</sub> flooding with ultrasonic. With the decrease of the MMP,

the displacement state changes from immiscible flooding to miscible flooding with the same displacement pressure. The full contact between CO<sub>2</sub> and crude oil improves its flow around and breakthrough, and the pore volume swept by CO<sub>2</sub> is larger, so the recovery efficiency of CO<sub>2</sub> flooding is improved.

#### 4. Conclusions

1. The crude oil's viscosity is reduced by 39%, 8 h after ultrasonic processing. The reason is that under the effect of ultrasonic, the unsaturated C-H bond in resin and asphaltene molecules in crude oil was destroyed and the saturated C-H bond was generated through hydrogenation reaction. The C-O bond was broken and the oxygen atom was replaced by a hydrogen atom to form a C-H bond. The C≡C bond was destroyed to form the C=C bond in aromatic rings and olefins. Under the influence of ultrasonic cavitation, the mole fraction of C<sub>25+</sub> molecules decreases with the destruction and recombination of these chemical bonds, while the mole fraction of C<sub>12-24</sub> molecules increases, indicating that macromolecules such as resin and asphaltene are decomposed into small molecules with relatively small carbon atoms, resulting in the decrease of their contents by 13.7% and 2.2%, respectively.

2. As the viscosity of crude oil decreased and the mole fraction of C<sub>12-24</sub> increased after ultrasonic treatment for 8 h, the MMP of the CO<sub>2</sub>-oil system decreased from 15.9 MPa to 14.8 MPa in the thin tube experiment, and the MMP calculated by the mixing-cell method decreased from 16.7 MPa to 15.7 MPa.

3. The displacement pressure is stable at 15 MPa, and the reduction of the MMP promoted the miscible phase of the CO<sub>2</sub>-oil system. Recovery increased by 11.7% from 54.3% without ultrasonic to 65.9% with ultrasonic. This result indicates that the ultrasonic-assisted CO<sub>2</sub> flooding can effectively reduce the MMP and improve the recovery.

**Author Contributions:** Conceptualization, H.W. and L.T.; methodology, H.W.; validation, Z.L.; resources, C.H.; data curation, L.J.; writing—original draft preparation, H.W.; writing—review and editing, K.Z.; visualization, X.C.; project administration, L.T. All authors have read and agreed to the published version of the manuscript.

**Funding:** This research was funded by National Natural Science Foundation of China (Grant No.: 51974329).

**Institutional Review Board Statement:** Not applicable.

**Informed Consent Statement:** Not applicable.

**Data Availability Statement:** Not applicable.

**Acknowledgments:** We thank Liam Cagney for English editing.

**Conflicts of Interest:** The authors declare no conflict of interest.

#### References

1. Dara, S.; Lindstrom, M.; English, J.; Bonakdarpour, A.; Wetton, B.; Wilkinson, D.P. Conversion of saline water and dissolved carbon dioxide into value-added chemicals by electro dialysis. *J. CO<sub>2</sub> Util.* **2017**, *19*, 177–184. [[CrossRef](#)]
2. Abbasi, J.; Ghaedi, M.; Riazi, M. A new numerical approach for investigation of the effects of dynamic capillary pressure in imbibition process. *J. Pet. Sci. Eng.* **2018**, *162*, 44–54. [[CrossRef](#)]
3. Huang, X.; Qi, Z.; Yan, W.; Yuan, Y.; Tian, J.; Qin, T. Functions of capillary pressure and dissolution in the CO<sub>2</sub> flooding process in low permeability reservoirs. *J. Pet. Explor. Prod. Technol.* **2020**, *10*, 1881–1890. [[CrossRef](#)]
4. Min, B.; Mamoudou, S.; Dang, S.; Tinni, A.; Sondergeld, C.; Rai, C. Comprehensive experimental study of huff-n-puff enhanced oil recovery in eagle ford: Key parameters and recovery mechanism. In Proceedings of the SPE Symposium on Improved Oil Recovery, v 2020-August, Society of Petroleum Engineers—SPE Improved Oil Recovery Conference 2020, IOR 2020, Tulsa, OK, USA, 31 August–4 September 2020; Society of Petroleum Engineers (SPE): Tulsa, OK, USA, 2020. ISBN 13 9781613997055.
5. Su, X.; Yue, X. Mechanism study of the relation between the performance of CO<sub>2</sub> immiscible flooding and rock permeability. *J. Pet. Sci. Eng.* **2020**, *195*, 107891. [[CrossRef](#)]
6. Gao, C.; Zhao, M.; Wang, J.; Zong, C. Performance and gas breakthrough during CO<sub>2</sub> immiscible flooding in ultra-low permeability reservoirs. *Pet. Explor. Dev.* **2014**, *41*, 88–95. [[CrossRef](#)]

7. Hao, S.; Yang, Z.; Li, X.; Peng, Y.; Lin, M.; Zhang, J.; Dong, Z. CO<sub>2</sub>-responsive agent for restraining gas channeling during CO<sub>2</sub> flooding in low permeability reservoirs. *Fuel* **2021**, *292*, 120306.
8. Wang, Y.; Shang, Q.; Zhou, L.; Jiao, Z. Utilizing macroscopic areal permeability heterogeneity to enhance the effect of CO<sub>2</sub> flooding in tight sandstone reservoirs in the Ordos Basin. *J. Pet. Sci. Eng.* **2021**, *196*, 107633. [[CrossRef](#)]
9. Chen, X.; Li, Y.; Tang, X.; Qi, H.; Sun, X.; Luo, J. Effect of gravity segregation on CO<sub>2</sub> flooding under various pressure conditions: Application to CO<sub>2</sub> sequestration and oil production. *Energy* **2021**, *226*, 120294.
10. Zhao, Y.; Fan, G.; Song, K.; Li, Y.; Chen, H.; Sun, H. The experimental research for reducing the minimum miscibility pressure of carbon dioxide miscible flooding. *Renew. Sustain. Energy Rev.* **2021**, *145*, 111091. [[CrossRef](#)]
11. Zhang, K.; Jia, N.; Zeng, F.; Li, S.; Liu, L. A review of experimental methods for determining the oil-gas minimum miscibility pressures. *J. Pet. Sci. Eng.* **2019**, *183*, 106366. [[CrossRef](#)]
12. Chen, H.; Zhang, C.; Jia, N.; Ian, D.; Yang, S.; Yang, Y. A machine learning model for predicting the minimum miscibility pressure of CO<sub>2</sub> and crude oil system based on a support vector machine algorithm approach. *Fuel* **2021**, *290*, 120048. [[CrossRef](#)]
13. Ge, D.; Cheng, H.; Cai, M.; Zhang, Y.; Dong, P. A new predictive method for CO<sub>2</sub>-Oil minimum miscibility pressure. *Geofluids* **2021**, *2021*, 8868529. [[CrossRef](#)]
14. Zhang, K.; Meng, Z.; Liu, L. Factorial two-stage analyses of parameters affecting the oil-gas interface and miscibility in bulk phase and nanopores. *J. Colloid Interface Sci.* **2019**, *555*, 740–750. [[CrossRef](#)] [[PubMed](#)]
15. Zhang, K.; Jia, N.; Li, S.; Liu, L. Thermodynamic phase behaviour and miscibility of confined fluids in nanopores. *Chem. Eng. J.* **2018**, *351*, 1115–1128. [[CrossRef](#)]
16. Gunde, A.C.; Bera, B.; Mitra, S.K. Investigation of water and CO<sub>2</sub> (carbon dioxide) flooding using micro-CT (micro-computed tomography) images of Berea sandstone core using finite element simulations. *Energy* **2010**, *35*, 5209–5216. [[CrossRef](#)]
17. Song, Z.; Li, Z.; Yu, C. D-optimal design for rapid assessment model of CO<sub>2</sub> flooding in high water cut oil reservoirs. *J. Nat. Gas Sci. Eng.* **2014**, *21*, 764–771. [[CrossRef](#)]
18. Choubineh, A.; Helalizadeh, A.; Wood, D.A. The impacts of gas impurities on the minimum miscibility pressure of injected CO<sub>2</sub>-rich gas-crude oil systems and enhanced oil recovery potential. *Pet. Sci.* **2019**, *16*, 117–126. [[CrossRef](#)]
19. Ghorbani, M.; Momeni, A.; Safavi, S.; Gandomkar, A. Modified vanishing interfacial tension(VIT) test for CO<sub>2</sub>-oil minimum miscibility pressure(MMP) measurement. *J. Nat. Gas Sci. Eng.* **2014**, *20*, 92–98. [[CrossRef](#)]
20. Zhang, C.; Xi, L.; Wu, P.; Li, Z. A novel system for reducing CO<sub>2</sub>-crude oil minimum miscibility pressure with CO<sub>2</sub>-soluble surfactants. *Fuel* **2020**, *281*, 118690. [[CrossRef](#)]
21. Yang, Z.; Wu, W.; Dong, Z.; Lin, M.; Zhang, S.; Zhang, J. Reducing the minimum miscibility pressure of CO<sub>2</sub> and crude oil using alcohols. *Colloids Surf. A—Physicochem. Eng. Asp.* **2019**, *568*, 105–112. [[CrossRef](#)]
22. Liu, J.; Sun, L.; Li, Z.; Wu, X. Experimental study on reducing CO<sub>2</sub>-Oil minimum miscibility pressure with hydrocarbon agents. *Energies* **2019**, *12*, 1975. [[CrossRef](#)]
23. Zhao, Y.; Song, K.; Fan, G.; Pi, Y.; Liu, L. The experiment for reducing the minimum miscible pressure of crude oil and carbon dioxide system with eater compounds. *Acta Pet. Sin.* **2017**, *38*, 1066–1072.
24. Wang, X.; Gu, Y. Oil recovery and permeability reduction of a tight sandstone reservoir in immiscible and miscible CO<sub>2</sub> flooding processes. *Ind. Eng. Chem. Res.* **2011**, *50*, 2388–2399. [[CrossRef](#)]
25. Cao, M.; Gu, Y. Physicochemical characterization of produced oils and gases in immiscible and miscible CO<sub>2</sub> flooding processes. *Energy Fuels* **2013**, *27*, 440–453. [[CrossRef](#)]
26. Cao, M.; Gu, Y. Oil recovery mechanisms and asphaltene precipitation phenomenon in immiscible and miscible CO<sub>2</sub> flooding processes. *Fuel* **2013**, *109*, 157–166. [[CrossRef](#)]
27. Mohamed, A.; Wu, Z.; Matthew, B.M.; Colin, D.W.; Nasser, S.A.; Liu, Y.; Renke, R.; Ali, S.; Xie, Q. Chemical-assisted minimum miscibility pressure reduction between oil and methane. *J. Pet. Sci. Eng.* **2021**, *196*, 108094.
28. Zhao, Y.; Fan, G.; Li, Y.; Zhang, X.; Chen, H.; Sun, H. Research for reducing minimum miscible pressure of crude oil and carbon dioxide and miscible flooding experiment by injecting citric acid isopentyl ester. *Arab. J. Chem.* **2020**, *13*, 9207–9215. [[CrossRef](#)]
29. Luo, H.; Zhang, Y.; Fan, W.; Nan, G.; Li, Z. Effects of the non-ionic surfactant (CiPOj) on the interfacial tension behavior between CO<sub>2</sub> and crude oil. *Energy Fuels* **2018**, *32*, 6708–6712. [[CrossRef](#)]
30. Bjorndalen, N.; Islam, M.R. The effect of microwave and ultrasonic irradiation on crude oil during production with horizontal well. *J. Pet. Sci. Eng.* **2004**, *43*, 139–150. [[CrossRef](#)]
31. Mohsin, M.; Meribout, M. Oil–water de-emulsification using ultrasonic technology. *Ultrason. Sonochem.* **2015**, *22*, 573579. [[CrossRef](#)]
32. Abramov, V.O.; Abramova, A.V.; Bayazitov, V.M.; Altunina, L.K.; Gerasin, A.S.; Pashin, D.M.; Mason, T.J. Sonochemical approaches to enhanced oil recovery. *Ultrason. Sonochem.* **2015**, *25*, 76–81. [[CrossRef](#)]
33. Abramov, V.O.; Mullakaev, M.S.; Abramova, A.V.; Esipov, I.B.; Mason, T.J. Ultrasonic technology for enhanced oil recovery from failing oil wells and the equipment for its implementation. *Ultrason. Sonochem.* **2013**, *20*, 1289–1295. [[CrossRef](#)]
34. Hamidi, H.; Mohammadian, E.; Asadullah, M.; Azdarpour, A.; Rafati, R. Effect of ultrasound radiation duration on emulsification and demulsification of paraffin oil and surfactant solution/brine using hele-shaw models. *Ultrason. Sonochem.* **2015**, *6*, 428–436. [[CrossRef](#)]
35. Hamidi, H.; Rafati, R.; Junin, R.; Manan, M.; Busra, N. A technique for evaluating the oil/heavy-oil viscosity changes under ultrasound in a simulated porous medium. *Ultrasonics* **2013**, *54*, 655–662. [[CrossRef](#)] [[PubMed](#)]

36. Mohammadian, E.; Junin, R.; Rahmani, O. Effects of sonication radiation on oil recovery by ultrasonic waves stimulated water-flooding. *Ultrasonics* **2013**, *53*, 607–614. [[CrossRef](#)] [[PubMed](#)]
37. Hossein, H.; Amin, S.H.; Erfan, M.; Roozbeh, R.; Amin, A.; Panteha, G.; Peter, O.; Tobias, N.; Aaron, Z. Ultrasound-assisted CO<sub>2</sub> flooding to improve oil recovery. *Ultrason. Sonochem.* **2017**, *35*, 243–250.
38. Czarnota, R.; Janiga, D.; Stopa, J.; Wojnarowski, P.; Kosowski, P. Minimum miscibility pressure measurement for CO<sub>2</sub> and oil using rapid pressure increase method. *J. CO<sub>2</sub> Util.* **2017**, *21*, 156–161. [[CrossRef](#)]
39. Czarnota, R.; Janiga, D.; Stopa, J.; Wojnarowski, P. Determination of minimum miscibility pressure for CO<sub>2</sub> and oil system using acoustically monitored separator. *J. CO<sub>2</sub> Util.* **2017**, *17*, 32–36. [[CrossRef](#)]
40. Ren, B.; Duncan, I.J. Maximizing oil production from water alternating gas (CO<sub>2</sub>) injection into residual oil zones: The impact of oil saturation and heterogeneity. *Energy* **2021**, *222*, 119915. [[CrossRef](#)]
41. Gopinath, R.; Dalai, A.K.; Adjaye, J. Effects of ultrasound treatment on the upgradation of heavy oil. *Energy Fuels* **2006**, *20*, 271–277. [[CrossRef](#)]
42. Liu, J.; Yang, F.K.; Xia, J.Y.; Wu, F.P.; Pu, C.S. Mechanism of ultrasonic physical-chemical viscosity reduction for different heavy oils. *ACS Omega* **2021**, *6*, 2276–2283. [[CrossRef](#)]
43. Chen, B.; Han, X.X.; Jiang, X.M. In situ FTIR analysis of the evolution of functional groups of oil shale during pyrolysis. *Energy Fuels* **2016**, *30*, 5611–5616. [[CrossRef](#)]
44. Shaw, A.; Zhang, X.L. Density functional study on the thermal stabilities of phenolic bio-oil compounds. *Fuel* **2019**, *225*, 115732. [[CrossRef](#)]
45. Wartini, N.; Brendan, P.M.; Budiman, M. Rapid assessment of petroleum-contaminated soils with infrared spectroscopy. *Geoderma* **2017**, *289*, 150–160.
46. Zhang, W.; Ning, Z.; Cheng, Z.; Wang, Q.; Wu, X.; Huang, L. Experimental investigation of the role of DC voltage in the wettability alteration in tight sandstones. *Langmuir* **2020**, *36*, 11985–11995. [[CrossRef](#)]
47. Lee, Y.; Chung, H.; Kim, N. Spectral range optimization for the near-infrared quantitative analysis of petrochemical and Petroleum products: Naphtha and gasoline. *Appl. Spectrosc.* **2006**, *60*, 892–897. [[CrossRef](#)]
48. Galán-Freyre, N.J.; Ospina-Castro, M.L.; Medina-González, A.R.; Villarreal-González, R.; Hernández-Rivera, S.P.; Pacheco-Londoño, L.C. Artificial intelligence assisted mid-infrared laser spectroscopy in situ detection of petroleum in soils. *Appl. Sci.* **2020**, *10*, 1319. [[CrossRef](#)]
49. Cao, M.; Gu, Y. Temperature effects on the phase behaviour, mutual interactions and oil recovery of a light crude oil–CO<sub>2</sub> system. *Fluid Phase Equilibria* **2013**, *356*, 78–89. [[CrossRef](#)]
50. Liao, C.; Liao, X.; Chen, J.; Ye, H.; Chen, X.; Wang, H. Correlations of minimum miscibility pressure for pure and impure CO<sub>2</sub> in low permeability oil reservoir. *J. Energy Inst.* **2014**, *87*, 208–214. [[CrossRef](#)]
51. Lai, F.; Li, Z.; Hu, X. Improved minimum miscibility pressure correlation for CO<sub>2</sub> flooding using various oil components and their effects. *J. Geophys. Eng.* **2017**, *14*, 331–340. [[CrossRef](#)]
52. Zhang, K.; Jia, N.; Liu, L. CO<sub>2</sub> storage in fractured nanopores underground: Phase behaviour study. *Appl. Energy* **2019**, *238*, 911–928. [[CrossRef](#)]
53. Holm, L.W.; Josendal, V.A. Effect of oil composition on miscible-type displacement by carbon dioxide. *Soc. Pet. Eng. J.* **1982**, *22*, 87–98. [[CrossRef](#)]
54. Chen, H.; Li, B.; Ian, D.; Moayad, E.; Liu, X. Empirical correlations for prediction of minimum miscible pressure and near-miscible pressure interval for oil and CO<sub>2</sub> systems. *Fuel* **2020**, *278*, 118272. [[CrossRef](#)]
55. Chen, G.; Fu, K.; Liang, Z.; Teerawat, S.; Li, C.; Paitoon, T.; Raphael, I. The genetic algorithm based back propagation neural network for MMP prediction in CO<sub>2</sub>-EOR process. *Fuel* **2014**, *126*, 202–212. [[CrossRef](#)]
56. Chen, G.; Gao, H.; Fu, K.; Zhang, H.; Liang, Z.; Paitoon, T. An improved correlation to determine minimum miscibility pressure of CO<sub>2</sub>–Oil system. *Green Energy Environ.* **2018**, *5*, 97–104. [[CrossRef](#)]
57. Zhang, K.; Gu, Y. Two different technical criteria for determining the minimum miscibility pressures (MMPs) from the slim-tube and coreflood tests. *Fuel* **2015**, *161*, 146–156. [[CrossRef](#)]
58. Zhang, K.; Gu, Y. New qualitative and quantitative technical criteria for determining the minimum miscibility pressures (MMPs) with the rising-bubble apparatus (RBA). *Fuel* **2016**, *175*, 172–181. [[CrossRef](#)]
59. Dang, S.; Sondergeld, C.; Rai, C. Interpretation of Nuclear-Magnetic-Resonance Response to Hydrocarbons: Application to Miscible Enhanced-Oil-Recovery Experiments in Shales. *SPE Reserv. Eval. Eng.* **2019**, *22*, 302–309. [[CrossRef](#)]